

†67 68 69 70 71

# Evaluation of the Virtual Crystal Approximation for Predicting Alloy Phonon Properties and Thermal Conductivity

Jason M. Larkin<sup>1</sup> and A. J. H. McGaughey<sup>1,\*</sup>

<sup>1</sup>*Department of Mechanical Engineering*

*Carnegie Mellon University*

*Pittsburgh, PA 15213*

(Dated: February 26, 2013)

## Abstract

The virtual crystal approximation for mass disorder is evaluated by examining two model alloy systems: Lennard-Jones argon and Stillinger-Weber silicon. In both cases the perfect crystal is alloyed with a heavier mass species up to equal concentration and phonon frequencies, lifetimes and group velocities and thermal conductivity are predicted. These two alloy systems have different ranges of phonon frequencies, lifetimes. For Stillinger-Weber silicon, the virtual crystal approximation predicts phonon properties and thermal conductivity in reasonably good agreement with molecular dynamics-based methods. For Lennard-Jones argon, the virtual crystal approximation underpredicts the high-frequency phonon lifetimes, leading to an underprediction of its thermal conductivity. Resolution of this underprediction is achieved by considering methods that treat the disorder explicitly.

## I. INTRODUCTION

Disordered materials (i.e., alloys and amorphous solids) are used in applications ranging from semiconducting devices to thermally insulating barriers due to their low thermal conductivities.(cite) An alloy is a lattice composed of multiple species which are spatially random (e.g. isotopic germanium).<sup>1</sup> Alloying (creating a disordered lattice) remains an effective method to reduce the thermal conductivity while maintaining good electrical transport properties.(cite) For example, reducing the thermal conductivity of thermoelectric materials can improve the efficiency of thermoelectric devices.<sup>2-4</sup>

Theoretical predictions for the thermal conductivity of disordered lattices dates back to the work of Abeles, who showed that mass and strain disorder dominate the thermal resistivity of Si-Ge and (Ga,In)-As alloys, respectively.<sup>5</sup> The Abeles theory assumed that the vibrations in the alloys were phonons, delocalized propagating modes, whose properties were computed assuming the disorder was a perturbation. Except for low-frequency (long-wavelength) modes, it is not clear which vibrational modes are phonon-like in alloys with arbitrary disorder.

In the case of dielectrics, almost all of the heat is conducted by the vibrational modes of the system. Understanding how these vibrations contribute to thermal transport is crucial for predicting the thermal conductivity of ordered and disordered lattices. Accurately predicting the thermal conductivity of a dielectric or semiconducting material requires the properties from the full spectrum of vibrational modes.<sup>6-8</sup> Accurate predictions of these properties for bulk systems can be made with anharmonic lattice dynamics (ALD) theory using *ab initio* calculations.<sup>4,9-14</sup> However, computational costs limit the size of computational cells in *ab initio* calculations to be less than 100 atoms, making it difficult to explicitly incorporate the effects of disorder.<sup>4,10,11,15,16</sup>

Recently, work using *ab initio* calculations, anharmonic lattice dynamics (ALD), and the virtual crystal (VC) approximation predicted phonon mode frequencies, lifetimes and group velocities of defected materials with relatively large (order 100 W/m-K<sup>10,11</sup>) and small (order 1 W/m-K<sup>4</sup>) thermal conductivities that compare well with experimental measurements. Under the VC approximation, the disordered solid is replaced with a perfect virtual crystal with properties equivalent to an averaging over the disorder (e.g., mass or bond strength).<sup>5</sup> The use of ALD with the VC approximation (referred to herein as VC-ALD) can base all

calculations on a small unit cell with averaged properties and treat the effects of intrinsic and disorder scattering as perturbations.<sup>1,4,5,10</sup> No comprehensive study has been performed to assess the applicability of this perturbative approach for a range of disorder (varying alloy concentrations, Section II B) using multiple predictive methods and test systems to test the self-consistency of the VC approximation.

The goal of this work is to investigate the use of the VC approximation for predicting vibrational mode properties and thermal conductivity of alloys by a detailed comparison of three predictive methods: (i) Molecular Dynamics (MD)-based normal mode decomposition (NMD, Section III C 1), (ii) MD-based green-kubo (GK, Section IV ), and (iii) VC-ALD (Section III C 2). Using computationally-cheap empirical potentials for argon<sup>17</sup> and silicon<sup>18</sup>, we study the effects of disorder explicitly. For both LJ argon and SW silicon, the perfect lattice is disordered with a heavier mass species up to equal concentration ( $c = 0.5$ ), spanning a range of perturbative to large disorder. By spanning this range, the limits of the perturbative models are examined.

We predict the phonon mode properties of the VC: frequencies (Section III), group velocities (Section III B ), and lifetimes (Section III C), and use them to predict thermal conductivity (Section IV). The breakdown of the perturbative VC-ALD method is examined (Section III C 2), and a simple guideline is suggested by the AF theory (Section III D), which predicts the thermal transport properties of the vibrations of the explicitly disordered lattices.

## II. THEORETICAL AND MODELING FORMULATION

### A. Thermal Conductivity Predictions

To predict the thermal conductivity of disordered lattices, one begins with the theory for a perfect lattice. For a perfect lattice, all vibrational modes are phonon modes, which by definition are delocalized, propagating plane waves.<sup>6</sup> Using the single-mode relaxation time approximation<sup>6</sup> to solve the Boltzmann transport equation<sup>19</sup> gives an expression for thermal conductivity,

$$k_{ph,\mathbf{n}} = \sum_{\boldsymbol{\kappa}} \sum_{\nu} c_{ph}(\boldsymbol{\kappa}) v_{g,\mathbf{n}}^2(\boldsymbol{\kappa}) \tau(\boldsymbol{\kappa}) . \quad (1)$$

Here,  $\kappa$  is the wavevector and  $\nu$  labels the phonon polarization. The phonon mode has frequency  $\omega(\kappa)$ ,  $c_{ph}(\kappa)$  is the phonon volumetric specific heat,  $v_{g,n}(\kappa)$  is the component of the group velocity vector in direction  $\mathbf{n}$ , and  $\tau(\kappa)$  is the phonon lifetime.

The SMRT approximation has been shown to be accurate for SiGe alloys and lower thermal conductivity materials, while larger conductivity materials such as GaN and Diamond require a full iterative solution to the BTE for more accurate predictions.<sup>9–11</sup> For the cubic lattices considered in this work, the lattices and the components of their thermal conductivity are cubically symmetric, so that we refer to  $k_{ph}$  as a scalar thermal conductivity. This is also true for the disordered lattices in the infinite size limit. Since MD simulations are classical and obey Maxwell-Boltzmann statistics,<sup>20</sup> the volumetric specific heat is  $k_B/V$  per mode in the harmonic limit, where  $V$  is the system volume. This approximation has been shown to be valid for LJ argon and SW silicon and is used in this work so that direct comparisons can be made between methods.<sup>21</sup>

For disordered systems, the vibrational modes of the system are no longer pure plane-waves (phonon modes), except in the low-frequency (long-wavelength) limit. The Allen-Feldman (AF) theory computes the contribution of diffusive, non-propagating modes to vibrational conductivity.<sup>22</sup> In the AF theory, the thermal conductivity is written as

$$k_{AF} = \sum_{modes} \frac{k_B}{V} D_{AF}(\omega), \quad (2)$$

where  $D_{AF}$  is the mode-specific thermal diffusivity of disordered vibrational modes defined at the wavevector [000].

In this high-scatter (HS) limit, the AF thermal conductivity prediction is

$$k_{AF,HS} = \frac{k_B}{V_b} b v_s a, \quad (3)$$

where  $V_b$  is the volume of the unit cell,  $v_s$  is the branch-averaged sound speed, and  $a$  is the lattice constant.<sup>23</sup> The relative contribution of both phonons and diffusons to the total vibrational conductivity has been estimated to be approximately equal for a-Si,<sup>24</sup> while earlier studies find that  $k_{ph}$  is substantially less.<sup>25</sup> While studies have been performed on alloying the amorphous phase, the AF theory has not been applied to disordered lattices.<sup>7</sup> In the current study of disordered lattices, the AF theory predictions provide a lower limit for the contribution of a given vibrational mode within the computational framework of the VC approximation. This is essential given the computational cost of the AF theory (Section ).

## B. Virtual Crystal Approximation

Under the Virtual Crystal (VC) approximation, the disordered solid is replaced with a perfect virtual crystal with properties equivalent to an averaging over the disorder (e.g., mass or bond strength).<sup>5</sup> Abeles first introduced the idea of using a VC to replace a disordered one, computing the thermal conductivity of SiGe, (Ga,In)As and In(As,P) alloys using Klemens-Callaway theory<sup>26–28</sup> and adjustable phenomenological fitting parameters to compare favorably with experimental results. The Abeles theory is conceptually simple, treating both disorder and anharmonicity as perturbations and expressing the thermal conductivity as a closed-form analytical function of the bulk material properties.<sup>5</sup> While good agreement between predictions and experimental measurements was found for SiGe and (Ga,In)As, deviations from the Abeles theory were observed for In(As,P) alloys at large concentrations, which was attributed to the high mass ratio of 3.7 for InP.<sup>5</sup>

While the Abeles theory is valid for perturbative disorder, its use leads to good agreement with several experimental and computational results for systems with a range of disorder. Cahill and co-workers found that conductivity reduction in dilute Ge-doped Si epitaxial layers can be explained by mass perturbative disorder.<sup>29,30</sup> The effect of bond and mass disorder was investigated computationally by Skye and Schelling for SiGe<sup>31</sup>, where it was shown that mass disorder is the dominant scattering mechanism. While the mass ratio is large ( $m_{Ge}/m_{Si} = 2.6$ ), the overall disorder strength is determined by both the mass ratio and the alloy concentration (Section III C 2). As little as  $6.2 \times 10^{19} cm^{-3}$  Ge is enough to reduce the thermal conductivity of Si by almost a factor of 2.<sup>29</sup> In the case of  $Ni_{0.55}Pd_{0.45}$ , with large mass disorder and concentration ( $m_{Pd}/m_{Ni} \approx 2$ ), good agreement is seen using the VC approach.<sup>32</sup> Given these experimental results, it is unclear what limitations exist using the VC approach for arbitrary disorder.

Computational results using the VC-ALD method for high thermal conductivity alloys show good to excellent agreement with experimental results for small and large concentrations.<sup>10,11</sup> These VC-ALD computations use *ab initio* methods to predict the mode-specific phonon properties of the VC. Unlike the phenomenological Abeles theory, the VC-ALD predicts thermal conductivity by summing over the whole spectrum of mode-specific phonon properties, where intrinsic and defect phonon scattering are treated as perturbations (Section ).(cite) Lindsay and Broido found good agreement with VC-ALD and experiment for

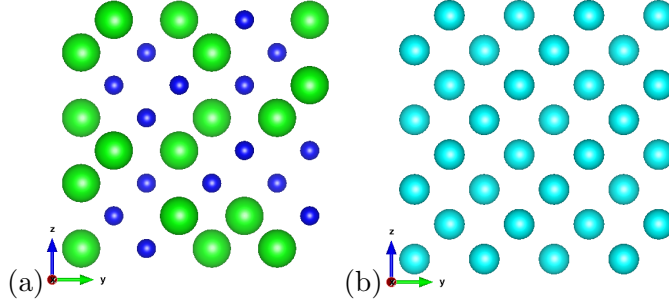


FIG. 1: (a) view of an explicitly disordered supercell of Si and “heavy” Si ([100] direction into the paper).<sup>34</sup> (b) view of the equivalent VC supercell with an average mass of the explicitly disordered Si and “heavy” Si supercell (b). Sphere size represents increasing mass only, no bond disorder is considered. In this work, calculations for LJ Ar and SW Si which use the VC approximation are based off of the conventional cubic unit cells (Section II C)

isotopically defected GaN with relatively small concentrations.<sup>10</sup> Garg used ab initio calculations with VC-ALD to predict the thermal conductivity of SiGe alloys for all concentrations, obtaining excellent agreement with experiment.<sup>11</sup> Isotopically defected GaN and SiGe alloys have relatively large thermal conductivities.(cite) In particular, the conductivity of SiGe alloys is significantly larger than that of the high scatter limit, which assumes that all vibrations scatter over a distance of the lattice spacing.<sup>23</sup> For both experiment and numerical modeling, VC predictions tend to be accurate when the thermal conductivity is significantly above the high-scatter limit.<sup>5,10,11,23,29,30,32</sup>

A detailed study of low thermal conductivity materials PbTe<sup>12</sup> and PbTe/PbSe<sup>4</sup> alloys made predictions for the perfect systems in fair agreement with experiment, but experimental results lack for the alloys.<sup>33?</sup> Thus, there is a need to examine the perturbative approach of VC-ALD for large (SW silicon) and small (LJ argon) thermal conductivity alloys for perturbative and large disorder. While the computational studies discussed above were limited to VC-ALD because of ab initio calculation costs, we use computationally cheap empirical potentials to include disorder explicitly.

### C. Calculation and Simulation Details

Perfect and explicitly disordered lattice supercells are generated with atomic positions based on LJ argon’s FCC ( $n = 4$ ) and silicon’s diamond-FCC ( $n = 8$ ) cubic conventional unit cells, where  $n$  is the number of atoms in the unit cell. Supercells are built cubically with size  $N_0$ , where  $N_0$  refers to the number of repetitions of the unit cell in all 3 spatial directions. Supercells up to size  $N_0 = 12$  (6096 atoms) are used for the LJ argon calculations. For SW silicon,  $N_0 = 8$  (4096 atoms) is used for the MD-based NMD methods, and  $N_0 \leq 42$  (592704 atoms) for MD-based GK and VC-ALD. The ALD calculations were performed using an in-house code,<sup>35</sup> with all classical expressions to remain consistent with the classical MD-based methods NMD and GK.

Disorder is created by randomly specifying the masses of the atoms on the lattice. The composition of the lattices is labeled by  $m_{1-c}^i m_c^j$ , where  $m^i = 1$  and  $m^j = 3$  in LJ units for argon and  $m^i = m_{Si}$  and  $m^j = 2.6m_{Si}$  for SW silicon and “heavy silicon” (mass of germanium). Concentrations of  $c = 0.0, 0.05, 0.15$  and  $0.5$  are used. For SW silicon, the lattice constant  $a = 5.43\text{\AA}$  is used for all calculations, which brings the GK thermal conductivity predictions at 300K<sup>36,37</sup> into better agreement with VC-ALD predictions for bulk SW silicon.<sup>38</sup> For LJ argon, supercells are built using the zero-pressure finite-temperature lattice constants, which are  $a = 1.556$  ( $T=10$  K) and  $a = 1.580$  ( $T=40$  K) in LJ units.<sup>39</sup> For LJ argon, the variation of lattice constant with composition is small and ignored.(cite) The amorphous LJ phase, discussed in Section , was created by liquifying the crystal and instantly quenching by removing all kinetic energy. The resulting structure was then energy minimized and annealed in an  $NPT$  ensemble at zero pressure and  $T = 10$  K.(cite lammps)) The effective zero-pressure lattice constant of the amorphous phase at  $T=10$ K, based on the atomic density, is slightly larger ( $a = 1.585$ ).<sup>39</sup>

The MD simulations were performed using the package LAMMPS(cite lammps) by equilibrating in a  $NVT$  (constant number of atoms N, volume V, and temperature T) ensemble before calculating atomic positions and velocities in a  $NVE$  (constant number of atoms N, volume V and energy E) ensemble.(cite) For LJ argon, a cutoff of  $2.5\sigma$  was used, where  $\sigma = 3.4\text{\AA}$ . Statistical averaging is accomplished using 10 simulations with different initial velocities. MD simulation time steps of 4.285 and 0.5 fs were used for LJ argon and SW silicon. For the GK method, the heat current was computed every 10 time steps. It is important to

note that the same atomic trajectories are used for the NMD and GK methods.

The key to incorporating the effects of disorder explicitly are the use of large disordered supercells. However, the methods used in this work scale differently with the size of the supercell considered. The calculations in this work are trivially parallelizable except the MD simulations<sup>40</sup> and the eigenvalue solution of the Dynamical matrix.<sup>41</sup> Efficient MD codes scale linearly with the number of atoms in the system,  $N_a$ . However, the computational cost of using large supercells for MD simulation, particularly the large number of time steps required (on the order of  $10^5 - 10^7$  depending on the system(cite)), prohibit its use with typical *ab initio* methods such as plane-wave Density Functional Theory.(cite) The Gamma-NMD and AF theory require the solution of a large Dynamical matrix of size  $(3N_a)^2$ , which limits the system sizes considered.

To predict a bulk thermal conductivity, extrapolation is used by the finite-size scaling  $1/k(N_0) \propto 1/N_0$ . For VC-NMD and VC-ALD, the validity of the finite-size scaling requires the low frequency modes in the system be dominated by intrinsic scattering ( $\tau(\kappa_\nu) \propto \omega(\kappa_\nu)^{-2}$ ) and follow the Debye approximation with respect to  $v_{g,\mathbf{n}}$  and DOS  $D(\omega(\kappa_\nu))$ .<sup>13,14</sup> For LJ argon alloys, this requirement is satisfied for modest system sizes (for  $N_0 = 6$  to 12) so that both VC-NMD and VC-ALD predictions can be extrapolated to a bulk value. For SW silicon alloys, the thermal conductivity is dominated by low-frequency modes, so that large system sizes are needed to satisfy the extrapolation requirements and only GK and VC-ALD can be used ( $N_0 \leq 42$  in the present study, similar to the converged system sizes in<sup>37</sup>). This highlights the efficiency of the VC-ALD method which is necessary when computationally expensive *ab initio* methods are used (Section ).<sup>4,10,11,14,42,43</sup>

### III. VIBRATIONAL MODE PROPERTIES IN ALLOY SYSTEMS

#### A. VC and Gamma DOS

In this section, we examine the effect of explicit disorder by computing the density of states (DOS,  $D(\omega)$ ) for vibrational modes of disordered lattice supercells and their equivalent VCs. The frequencies are computed using harmonic lattice dynamics calculations with the package GULP.<sup>41</sup> For the VC, the allowed wavevectors are set by  $N_0$ , and each wavevector represents a finite volume of the crystal lattice's irreducible Brillouin zone (BZ).(cite mermin)

The symmetry properties of the BZ define a set of irreducible wavevectors, which are used to average the mode properties of the reducible wavevectors.(cite)

For the disordered supercells, the only allowed wavevector is the gamma-point (i.e.,  $\kappa = 0$ ). The DOS for the VC and the explicitly disordered supercells (referred to herein as Gamma) are shown in Fig. 2. The VC and Gamma DOS agree at low frequencies, where the Debye approximation predicts  $DOS \propto \omega^2$ .(cite) The Debye approximation underpredicts the the DOS at moderate frequency, which is due to the non-linear dispersion.(cite Mermin)

The increasing lattice mass with increasing concentration for the VC reduces the frequencies. The increasing lattice mass for the Gamma modes also reduces the frequencies. The effect of explicit disorder is seen at high frequencies by a broadening and a shift of the DOS to higher frequencies because of the explicit use of light atoms in the supercell. Duda et al observed similar high-frequency broadening effects in model LJ alloys.<sup>44</sup> Similar agreement at low frequencies was found in *ab initio* predictions for  $\text{Si}_c\text{Ge}_{1-c}$ ,<sup>11</sup> while Bouchard showed similar continuous behavior at low frequency for a- $\text{Si}_c\text{Ge}_{1-c}$ .<sup>45</sup> Based on the DOS, the vibrational modes of the explicitly disordered supercells at low frequencies are phonon-like, while the broadening of the DOS at high-frequency indicate that the vibrational modes may differ significantly from the high-frequency VC phonon modes.

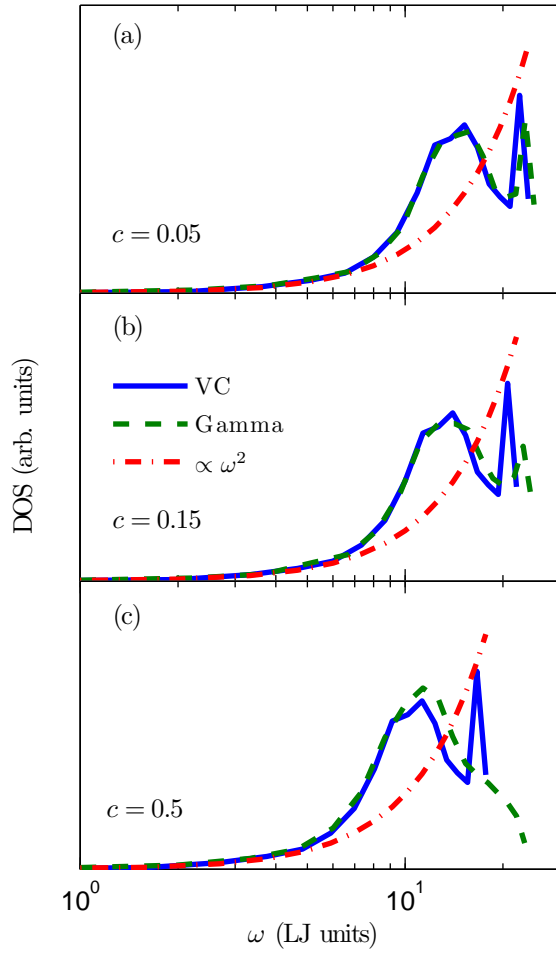


FIG. 2: Density of states (DOS) for modes calculated using the LJ FCC VC versus an explicitly mass disordered LJ FCC supercell (labeled Gamma) with varying mass concentration  $c$ . VC and Gamma show similar low frequency behavior for all  $c$ . For increasing  $c$ , the frequencies of both VC and Gamma decrease, while the high frequency DOS for Gamma spreads and reaches up to a higher maximum frequency because of the explicit disorder. The size of these supercells is  $N_0 = 12$  (see Section II C).

## B. Dispersion and Group Velocity

The group velocity vector in a VC is the gradient of the dispersion curves,

$$v_{g,\mathbf{n}}(\boldsymbol{\kappa}) = \frac{\partial\omega(\boldsymbol{\kappa})}{\partial\boldsymbol{\kappa}}. \quad (4)$$

We calculate the group velocities for the VC using finite differences and quasi-harmonic lattice dynamics.<sup>46</sup>

Except for the three acoustic branches (2 transverse, 1 longitudinal sound speeds), there is not an accepted method to predict the effective group velocity of a vibrational mode in a disordered system, although there have been attempts.<sup>23,24,44,47,48</sup> In the Cahill-Pohl (CP) model, the group velocity of all disordered modes is the sound speed,  $v_s$ .<sup>23</sup> Dispersion for a model disordered 1D system demonstrated the reduction of the frequency-dependent group velocities due to the zone-folding effect.<sup>44</sup>

Calculating the structure factor of the supercell Gamma modes is a method to test for the plane-wave character of disordered modes at a particular wavevector and polarization.<sup>8,25</sup> Feldman et al used the structure factor to predict an effective dispersion for a model of a-Si, but did not predict group velocities.<sup>25</sup> Volz and Chen used the dynamic structure factor to predict the dispersion of crystalline SW Si using MD simulation.<sup>49</sup>

The structure factor is defined as<sup>8</sup>

$$S^{L,T}(\boldsymbol{\kappa}) = \sum_{\nu} E^{L,T}(\boldsymbol{\kappa}) \delta(\omega - \omega(\boldsymbol{\kappa}=\mathbf{0})), \quad (5)$$

where  $E^T$  refers to transverse polarization and is defined as

$$E^L(\boldsymbol{\kappa}) = \left| \sum_{l,b} \hat{\boldsymbol{\kappa}} \cdot e(\boldsymbol{\kappa}=\mathbf{0} \ b) \exp[i\boldsymbol{\kappa} \cdot \mathbf{r}_0(l=b)] \right|^2 \quad (6)$$

and  $E^L$  refers to longitudinal polarization and is defined as

$$E^T(\boldsymbol{\kappa}) = \left| \sum_{l,b} \hat{\boldsymbol{\kappa}} \times e(\boldsymbol{\kappa}=\mathbf{0} \ b) \exp[i\boldsymbol{\kappa} \cdot \mathbf{r}_0(l=b)] \right|^2. \quad (7)$$

Here,  $\mathbf{r}_0(l=b)$  refers to the atomic positions of the mass disordered atoms in the supercells, which are still spatially ordered. Explicit disorder is accounted for in the mode frequencies  $\omega(\boldsymbol{\kappa}=\mathbf{0})$  and eigenvectors  $e(\boldsymbol{\kappa}=\mathbf{0} \ b)$ , which are calculated with  $\boldsymbol{\kappa} = \mathbf{0}$ .

Physically,  $S^{L,T}(\boldsymbol{\omega})$  represents the frequency spectrum required to create a wavepacket with a well-defined wavevector and polarization.<sup>8,25</sup> For a perfect lattice, the structure factor peaks are delta functions centered at the phonon mode frequencies, indicating they are pure plane-waves. The structure factors for LJ argon alloys are plotted in Fig. 3 for wavevectors along the [100] and [111] directions. With increasing disorder, the structure factor spreads in width, particularly at high frequencies because the modes are no longer pure plane-waves.

From Fig. 3, an effective dispersion can be extracted by locating the peaks in the structure factors at neighboring VC wavevectors, where the effects of polarization, virtual mass, and anisotropic dispersion can be observed. As the lattice VC mass becomes larger, the peaks in the structure factor shift to lower frequencies. The peaks in the structure factor are at slightly higher frequencies than the VC predicted frequencies by up to only %5. Similarly, good agreement is found with the disordered SW silicon lattice supercells (not shown), while the structure factors are more complicated because of the optical modes. Well-defined peaks at all wavevectors are most likely due to the lattice structure of the disordered systems studied in this work. Typically, the structure factor for amorphous materials has well-defined peaks only for small wavevector.<sup>8,25</sup>

Because of the good agreement between the VC predicted dispersion and the peaks in the structure factors from Fig. 3, we use the group velocities predicted by the VC dispersion for both LJ argon and SW silicon with the VC-NMD and VC-ALD calculations for consistency and simplicity. We will examine the validity of this choice of group velocity in Section III D.

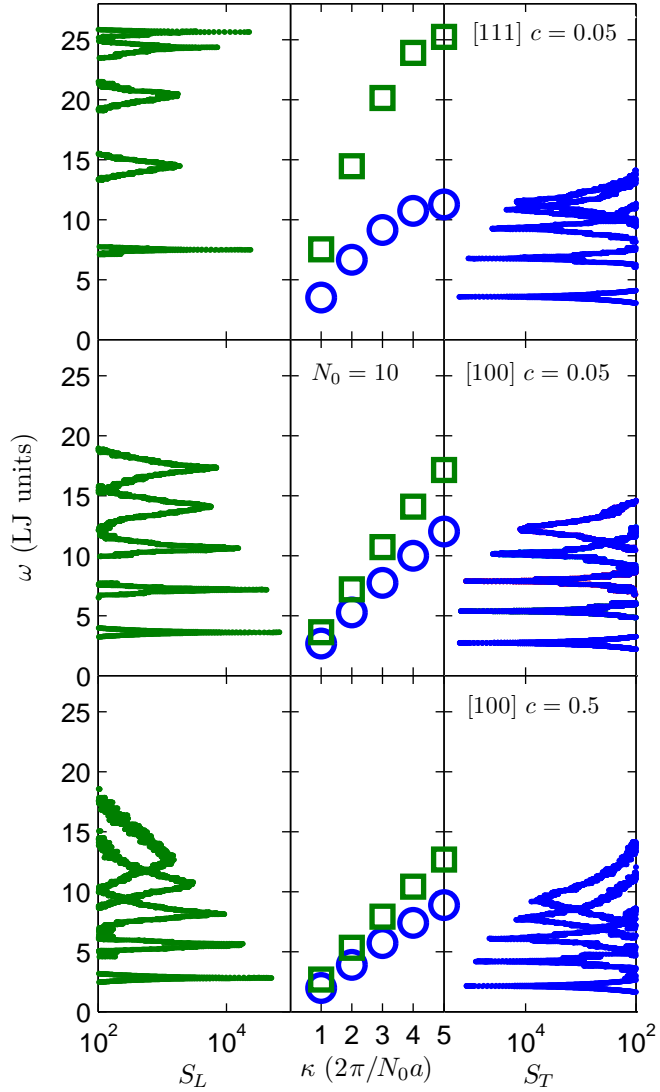


FIG. 3: Left and Right Panels: The structure factor for longitudinal ( $S_L$ ) and transverse ( $S_T$ ) polarizations along high symmetry directions ([100], [110] where  $\kappa = \pi/a[100]$  and  $a$  is the lattice constant ) of the mass disordered LJ argon supercells ( $N_0 = 10, c = 0.05, 0.5$ ). For increasing mass disorder  $c$ , there is a decrease in the center of the peaks and an increase in the peak linewidths. Center Panel: The VC predicted dispersion at the same wavectors used to calculate  $S_{L,T}$ .

### C. Lifetimes

#### 1. From VC-NMD and Gamma-NMD

Once the group velocities are predicted using the VC dispersion, the phonon mode lifetimes are required to predict the thermal conductivity using Eq. ((1)). As an alternative to the VC-ALD models for predicting phonon lifetimes, which are discussed in the next section, we first use the normal mode decomposition (NMD) method.<sup>35,50</sup> NMD maps the atomic trajectories (positions and velocities) of atoms in an MD simulation onto the vibrational normal mode coordinates,(cite)

$$q(\boldsymbol{\kappa}; t) = \sum_{\alpha, b, l}^{3, n, N} \sqrt{\frac{m_b}{N}} u_\alpha(l; t) e^*(\boldsymbol{\kappa}_\alpha^b) \exp[i\boldsymbol{\kappa} \cdot \mathbf{r}_0(l)] \quad (8)$$

and

$$\dot{q}(\boldsymbol{\kappa}; t) = \sum_{\alpha, b, l}^{3, n, N} \sqrt{\frac{m_b}{N}} \dot{u}_\alpha(l; t) e^*(\boldsymbol{\kappa}_\alpha^b) \exp[i\boldsymbol{\kappa} \cdot \mathbf{r}_0(l)]. \quad (9)$$

where  $\mathbf{r}_0(l)$  are the equilibrium positions of the atoms in the  $l$ th unit cell of the lattice supercell under the VC approximation. The total energy of a given vibrational mode is

$$E(\boldsymbol{\kappa}; t) = \frac{\omega(\boldsymbol{\kappa})^2}{2} q(\boldsymbol{\kappa}; t)^* q(\boldsymbol{\kappa}; t) + \frac{1}{2} \dot{q}(\boldsymbol{\kappa}; t)^* \dot{q}(\boldsymbol{\kappa}; t) \quad (10)$$

We perform NMD using the frequencies and eigenvectors from both the VC ( $\omega(\boldsymbol{\kappa})$ ,  $e(\boldsymbol{\kappa}_\alpha^b)$ ) and the Gamma supercell ( $\omega(\boldsymbol{\kappa}=\mathbf{0})$ ,  $e(\boldsymbol{\kappa}=\mathbf{0}_\alpha^b)$ ). The trajectories from these MD simulations are also used in the GK method (Section IV). For the NMD method (Section III C 1), the atomic positions and velocities were sampled at a rate dictated by the highest vibrational frequencies in the system, which can be estimated from harmonic lattice dynamics calcualtions (Section III A).

The MD simulations are performed using the package LAMMPS.<sup>40</sup> The lengths of the MD simulations were longer than 10 times the longest phonon lifetime in the system. These can be estimated a priori from the VC-ALD predicted phonon lifetimes. For LJ argon and SW silicon, the simulations were run using time steps of  $dt = 0.002$  LJ units and  $dt = 0.0005$  fs for  $2^{20}$  and  $2^{22}$  time steps and the atomic trajectories were sampled every  $2^8$  and  $2^4$  time steps, respectively. Ensemble averaging was performed using 10 independent initial randomized velocity distributions.

The normal vibrational mode lifetime is predicted using

$$\tau(\nu) = \int_0^\infty \frac{\langle E(\nu; t) E(\nu; 0) \rangle}{\langle E(\nu; 0) E(\nu; 0) \rangle} dt, \quad (11)$$

where the upper integration limit is much larger than the phonon lifetime.(cite) For normal modes of the lattice supercell, Eq. (11) is exact, but becomes an approximation when using non-exact normal modes to perform the mappings Eq.s (8) and (8). An effective lifetime can be predicted using Eq. (11), even for larger disorder ( $c = 0.5$ ) where the energy autocorrelations are more complicated but generally follow exponential decay (see Appendix A). The phonon frequency cannot be predicted using Eq. (11), so the mode frequencies are taken to be those predicted by the VC dispersion.

The lifetimes predicted using VC-NMD and Gamma-NMD are shown in Fig. 4 for LJ argon alloys at  $T = 10$  K. The range of frequencies of the modes for VC-NMD and Gamma-NMD differ slightly which is due to differences in the DOS (Fig. 2). For small intervals of frequency, there are a wider range of predicted lifetimes for Gamma-NMD. This is because there is no symmetry averaging of the mode properties, which is possible for the VC (Section III A). Lifetimes predicted by both VC-NMD and Gamma-NMD show scalings of  $\tau$  with frequency of  $\omega^{-2}$  at low frequency and  $\omega^{-4}$  and even faster for mid-range frequencies (Fig. 4). In general, the lifetimes predicted by both VC-NMD and Gamma-NMD are larger than the Ioffe-Regel (IR) limit,<sup>51</sup>

$$\tau = \frac{2\pi}{\omega}. \quad (12)$$

The physical interpretation of the IR limit is that of a mode which scatters in a time equal to its oscillation period, which seems to be a good lower-limit for the lifetimes predicted by VC-NMD and Gamma-NMD for LJ argon (Fig. 4) and VC-NMD for SW silicon (Fig. 8(a)).

The behavior at the highest frequencies, where  $\tau$  *constant*, is seen for both VC-NMD and Gamma-NMD, except at  $c = 0.5$  for VC-NMD. Since the existence of this characteristic (thought not exactly minimum) lifetime for LJ argon is demonstrated by both VC-NMD and Gamma-NMD, it is physically meaningful. There is, however, no theoretical prediction of this high-frequency behavior of the mode lifetime.<sup>23,52,53</sup>

Overall, good agreement is seen in the predicted lifetimes from VC-NMD and Gamma-NMD both in magnitude and trends. The use of the VC normal modes is an approximation which becomes worse as the concentration is increased (Appendix A). The only approximation associated with Gamma-NMD is the use of the harmonic lattice dynamics predicted

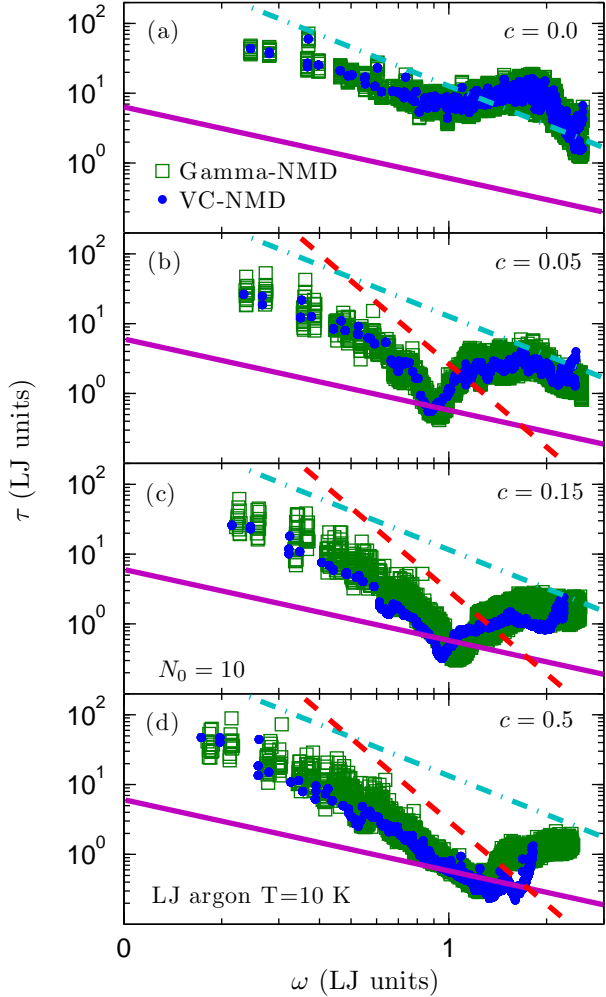


FIG. 4: Lifetimes predicted using VC-NMD and Gamma NMD from MD simulations of mass disordered lattice supercells (Section III C 1). Both  $\omega^{-2}$  and  $\omega^{-4}$  scalings can be observed at low frequencies, which are predicted by the perturbative models used for VC-ALD (Section III C 2). For both VC-NMD and Gamma NMD, most mode lifetimes are greater than the Ioffe-Regel limit  $\tau = 2\pi/\omega$ .<sup>51</sup> While there is more “noise” in the Gamma-NMD data (Section III C 1), the lifetime magnitudes and trends agree well, an important consideration when comparing VC-NMD and VC-ALD in Fig. 5 .

frequencies and eigenvectors to map the atomic trajectories from the fully anharmonic MD simulations, which has been shown to be valid at the low temperatures.<sup>35</sup> Based on the good agreement with Gamma-NMD, the lifetimes predicted by VC-NMD are used along with the VC predicted group velocities to predict thermal conductivity in Section IV.

## 2. From VC-ALD

Assuming intrinsic and disorder scattering mechanisms to operate independently, the effective phonon lifetime can be found using Matthiessen's rule(cite),

$$\frac{1}{\tau(\nu)} = \frac{1}{\tau_{p-p}(\nu)} + \frac{1}{\tau_{p-d}(\nu)}, \quad (13)$$

where  $\tau_{p-p}(\nu)$  accounts for intrinsic phonon-phonon scattering and  $\tau_{p-d}(\nu)$  accounts for defect scattering.

Phonon-phonon scattering ( $\tau_{p-p}(\nu)$ ) is typically treated using anharmonic perturbation theory (ALD) including only three-phonon processes.<sup>4,11,35</sup> It has been demonstrated that the effects of higher order phonon processes become important at high temperatures.<sup>35,54</sup> In this work, the intrinsic phonon lifetimes  $\tau_{p-p}(\nu)$  are predicted using the method described in<sup>35</sup>, with all classical expressions to remain consistent with the classical MD-based methods NMD and GK.

Using harmonic perturbation theory, Tamura derives a general expression for mass point defect scattering.<sup>1</sup> By considering the symmetry properties of the FCC lattices considered in this work (Section II C), it can be shown that<sup>1</sup>

$$\frac{1}{\tau_{p-d}(\nu)} = \frac{\pi}{2} g_2 \omega^2(\nu) D(\omega), \quad (14)$$

where  $D(\omega)$  is the density of states (Section III A) and

$$g_n = \sum_\mu c^\mu (1 - m^\mu / \bar{m}^\mu)^n. \quad (15)$$

Here,  $c^\mu$  is the concentration,  $m^\mu$  is the mass of the  $\mu$ -th species and  $\bar{m}^\mu$  is the average mass. Bond disorder can be accounted for using a similar expression with an average atomic radius or suitable scattering cross-section.<sup>26,27</sup> For the binary LJ argon and SW silicon alloys considered, there is one atom type in the unit cell with  $\mu = i, j$ , so that the alloying atom labeled by  $m_{1-c}^i$  can be considered to be an “isotope” of atom labeled  $m_c^j$ . This convention is appropriate because isotopic impurities create perturbative disorder,<sup>1</sup> while we consider the use of Eq. (14) for large disorder. To calculate the disordered lifetimes  $\tau_d(\nu)$ , it is necessary to broaden the  $\delta$  function using a Lorentzian function.

The lifetimes predicted by VC-ALD for LJ argon at  $T = 10$  K and  $c = 0.05$  are shown in Fig. 5 (a). At low frequencies where the density of states is Debye-like [ $D(\omega) \propto \omega^2$ , Fig.

2],  $\tau_{p-p}(\kappa)$  follows a general scaling of  $\omega^{-2}$ , which is due to intrinsic 3-phonon scattering processes.(cite) From Figs. 4 and 5 (a) , the scaling  $\tau \propto \omega^{-2}$  can be observed in the VC-NMD, Gamma-NMD and VC-ALD predicted results. Under the Debye-approximation , the phonon scattering due to mass point-defects is given by  $A\omega^{-4}$ , where  $A$  is a constant related to the unit cell volume, branch-averaged group velocity, and disorder coupling strength ( $g_2(b)$ , Eq. (15)). The frequency dependence ( $\omega^4$ ) is the same as Rayleigh scattering, which is valid at low frequency and observed in both the NMD (Fig. 4) and ALD (Fig. 5 (a)) predicted lifetimes. VC-ALD does not predict the behavior of the lifetimes at high frequency for LJ argon,  $\tau$  *constant*. From Fig. 5 (c), the thermal conductivity frequency spectrum demonstrates that the conductivities of LJ argon and its alloys are dominated by high frequency modes (Fig. 5 c).(cite) It can be seen that VC-ALD underpredicts the thermal conductivity at high-frequencies, precisely where the lifetimes are underpredicted by VC-ALD compared to VC-NMD.

The Tamura theory was developed to predict the reduction of lifetimes in isotopic Ge, which is only perturbatively disordered. The importance of n-order ( $n > 2$ ) interactions in the Tamura theory become important with increasing disorder strength  $g_n$  (Eq. (15)).<sup>1</sup> For isotopically-disordered Ge, the higher-order contributions were estimated to be negligible for all frequencies.<sup>1</sup> For LJ argon and the large concentrations and mass ratios considered in this work, the terms higher order terms are order 1 and larger at high frequencies. It is possible that higher-order interactions in the Tamura theory are responsible for the discrepancy of the lifetimes predicted by VC-NMD and Gamma-NMD versus VC-ALD at high frequency.

## D. Diffusivities

Once the group velocities and lifetimes are predicted, these can be used to predict the mode thermal diffusivity. For large disorder, only modes at low frequency have well-defined group velocities and lifetimes. At high frequencies it is not possible to specify a mode group velocity and lifetime independently,<sup>25,55</sup> and the mode thermal diffusivity must be considered.

In the classical harmonic limit, where the specific heat  $c_p(\nu) = k_B/V$ , a vibrational mode's contribution to thermal conductivity is determined by the mode thermal diffusivity. For phonons, the thermal diffusivity is

$$D_{ph,\mathbf{n}}(\nu) = v_{g,\mathbf{n}}(\nu) \tau(\nu). \quad (16)$$

For VC-NMD and VC-ALD,  $v_{g,\mathbf{n}}(\nu)$  is calculated from the VC dispersion (Section III B) so any differences in thermal diffusivity comes from the predicted lifetimes. The lower limit for phonon thermal diffusivity is  $D_{ph,\mathbf{n}}(\nu) \approx 0$  since the group velocities can approach zero for modes such as optical and those near the Brioullin zone boundaries.(cite)

In disordered systems, modes can transport heat by harmonic coupling due to disorder in the Allen-Feldman (AF) theory of diffusons.<sup>22</sup> In the high-scatter (HS) limit,(cite) the AF diffusivity of each mode is

$$D_{AF,HS} = \frac{1}{3}v_s a, \quad (17)$$

which leads to the AF,HS limit prediction for thermal conductivity, Eq. (3). The physical interpretation is all vibrational modes transport heat at the sound speed and scatter with a mean free path of the lattice spacing. As seen in Fig. 5 for LJ argon alloy  $c = 0.05$ , VC-NMD and VC-ALD predict from Eq. (16) a significant number of modes with  $D_{ph}(\nu) < D_{AF,HS}$ . This can lead to an underprediction of the total thermal conductivity (Section ).

While AF,HS model assumes a mode-independent thermal diffusivity, the AF theory is capable of predicting the mode specific diffusivities.<sup>7,7,25,56</sup> Since the AF theory is harmonic, mode diffusivities typically diverge as  $\omega \rightarrow 0$  because the vibrations are long-wavelength plane waves that weakly scattered by the disorder.<sup>57,58</sup> The mode-specific thermal diffusivities for the LJ argon amorphous phase are shown in Fig. 6. Except at the highest frequencies, the thermal diffusivity of all modes can be modeled using a mode-independent diffusivity of approximately  $D_{AF,HS}$ . Also shown in Fig. 6 are the AF predicted thermal diffusivities for

the explicitly disordered LJ argon superlattice and  $c = 0.5$ . While the AF theory is divergent in the low-frequency limit for lattices, the finite system size limits the thermal diffusivities of the lowest frequencies. The thermal diffusivity of all modes in the explicitly disordered lattice supercell are larger than  $D_{AF,HS}$ , except at the highest frequencies where they tend to zero as in the amorphous phase.(cite) This result supports the plausible lower-bound of the VC predicted phonon thermal diffusivity,  $D_{ph} \geq D_{AF,HS}$ .

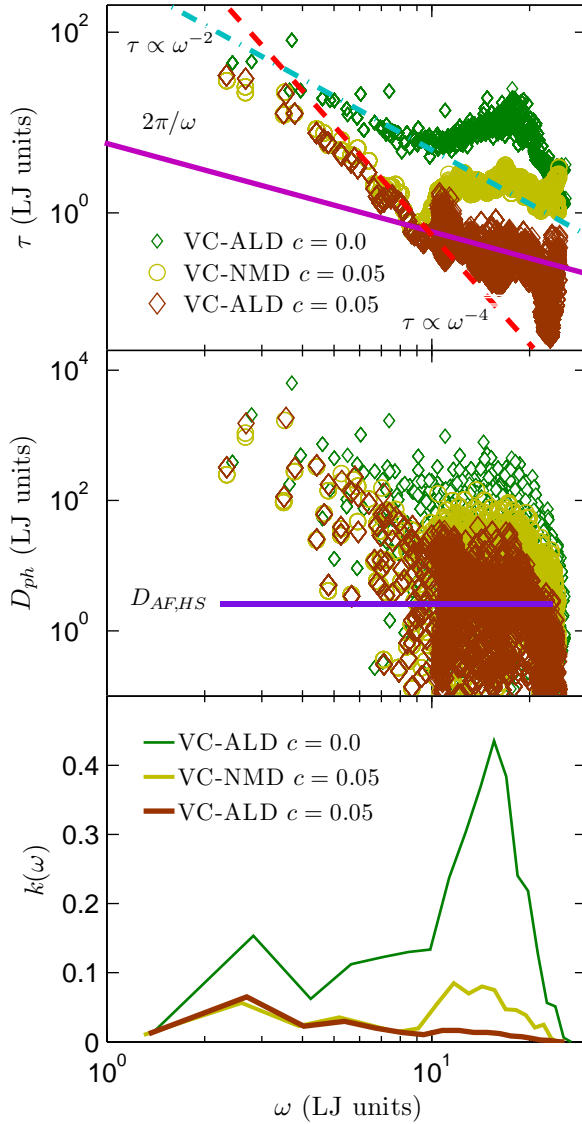


FIG. 5: (a) predicted lifetimes for VC modes using VC-NMD and VC-ALD for LJ argon ( $T = 10$  K,  $N_0 = 10$  and  $c = 0.05$ ). (b) predicted VC mode thermal diffusivities, compared to the AF,HS limit. (c) the thermal conductivity frequency spectrum, which is peaked at high frequency, in contrast to SW silicon (Fig 8).

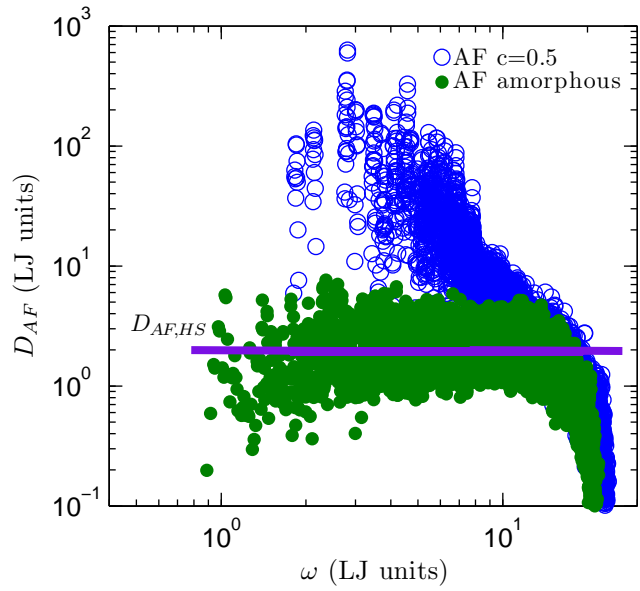


FIG. 6: AF theory predictions of disorded mode thermal diffusivities for LJ argon disorded lattice supercell and amorphous phase. The mode thermal diffusivities predicted for the disorded lattice supercell are all finite, except at the highest frequency where they tend to 0 as in the amorphous phase.

### E. Mode Properties Discussion

For disordered systems it is only possible to assign a unique lifetime and group velocity to a vibrational mode only in the low-frequency, propagating limit.<sup>25,55</sup> This implies that the VC predicted group velocities, particularly for  $v_g(\kappa) \ll v_s$  or  $v_g(\kappa) \approx 0$ , are an underprediction of the representative velocity scale for the thermal diffusivity of high-frequency modes in the disordered lattice. Predictions from model disordered systems demonstrates the existence of a plateau of the thermal diffusivity, which is consistent with the minimum phonon mean-free path hypothesis.<sup>59</sup> A minimum vibrational mean free path is used in most models of thermal transport in disordered materials.<sup>23,52,53</sup> However, the concept of a vibrational mean free path is only valid for low-frequency propagating modes in disordered systems.<sup>25</sup> The more fundamental property is the vibrational mode lifetime<sup>51</sup> and thermal diffusivity.<sup>7,8,22,25</sup>

VC-NMD and Gamma-NMD predicts lifetimes which are generally larger than the IR limit for LJ argon (Fig. 4). VC-ALD predicts essentially monotonically decreasing lifetimes with increasing frequency for both LJ argon (Fig. 5 (a)) Because VC-NMD and VC-ALD use the same predictions for  $v_g(\kappa)$ , the phonon mode diffusivities  $D_{ph}(\kappa)$  are underpredicted for VC-ALD compared to VC-NMD for LJ argon alloys. There are thus 2 underpredictions to consider when predicting the thermal conductivities: underprediction of the thermal diffusivity assuming the VC group velocities for VC-NMD and VC-ALD, and the underprediction of the mode lifetimes for LJ argon alloys by the VC-ALD perturbative models.

## IV. THERMAL CONDUCTIVITY PREDICTIONS

The thermal conductivity can now be predicted using the vibrational mode properties predicted by the VC-NMD and VC-ALD methods. Given the discussion of the VC-predicted mode properties in Section III E, it is necessary to implement a third method for predicting thermal conductivity. We choose the equilibrium MD-based green-kubo (GK) method(cite), which is a system-level method that does not predict any mode-specific properties. Thermal conductivities predicted by GK naturally capture the effects of whatever scattering mechanisms are present in the MD simulation without any assumptions.<sup>31,60,61</sup> For GK, the thermal conductivities are defined by the converged value of the integral of the heat current autocorrelation function for a given system size  $N_0$ .

For LJ argon, bulk thermal conductivity predictions are made for VC-NMD, VC-ALD, and GK using a finite simulation size extrapolation procedure (Section II C) and are shown in Fig. 7. For LJ argon, VC-NMD and VC-ALD underpredict the thermal conductivity compared to GK. The underprediction is only modest for VC-NMD, on the order of 20% or less for all concentrations. Based on the limit  $D_{AF,HS}$  (Eq. (17)), the thermal diffusivities predicted by Eq. (16) for VC-ALD and VC-NMD can be adjusted such that any mode with  $D_{ph} < D_{AF,HS}$  is given  $D_{ph} = D_{AF,HS}$ . The result of this adjustment, referred to as VC-NMD\* and VC-ALD\*, is shown in Fig. 7. The thermal conductivtiy predicted by VC-NMD\* is brought into agreement with GK by approximately 10% or less for all  $c$ . Combined with  $D_{AF,HS}$ , the VC-NMD predicted thermal diffusivities seem to be fair representations for the explicitly disordered modes present in the MD simulation.

The VC-ALD method underpredicts the thermal conductivity of LJ argon alloys, where the underprediction is worst for  $c = 0.05$ ,  $k_{VC-ALD}/k_{GK} = 0.56$  (error bars are on the order of the large symbol sizes in Fig. 7). By applying the high-scatter limit adjustment VC-ALD\*, the thermal conductivities are brought into marginally better agreement, worst for  $c = 0.05$ ,  $k_{VC-ALD^*}/k_{GK} = 0.65$ . The VC-ALD method fails to accurately predict the high-frequency mode thermal diffusivities for LJ argon alloys, which can be seen in Fig. 5 (b). Since the group velocities are the same for VC-NMD and VC-ALD, the underprediction of the high-frequency thermal diffusivities, and hence thermal conductivity, is due to the underpediction of the high-frequency mode lifetimes (Fig. 5 (a)). Thus the adjustment  $VC - ALD^*$  fails to bring VC-ALD into agreement with VC-NMD and GK.

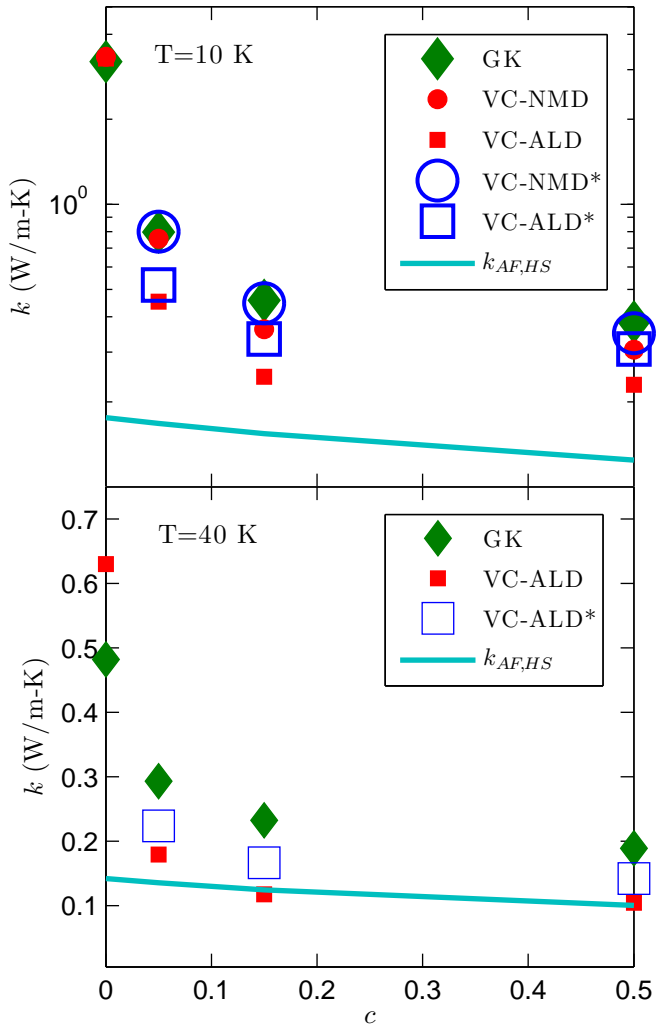


FIG. 7: (a) thermal conductivity predictions for LJ argon alloys at  $T=10\text{K}$  using the VC-NMD, VC-ALD, and GK methods. (b) (getting rid of this) thermal conductivity predictions at  $T=40\text{K}$

## V. SW SILICON

Because of the discrepancies between the VC-NMD and VC-ALD predicted mode properties and thermal conductivity for LJ argon alloys (Section ), we predict the mode properties and thermal conductivity for SW silicon alloys. Fig. 8 (a) shows the lifetimes predicted by VC-NMD and VC-ALD. VC-NMD predicts lifetimes which are generally larger than the IR limit for SW silicon alloys, similar to VC-NMD predictions for LJ argon (Fig. ). Unlike LJ argon, VC-NMD and VC-ALD lifetime predictions agree over most of the frequency spectrum, except at the highest frequencies where VC-ALD underpredicts. While there is a plateau of the VC-NMD predicted mode lifetimes for LJ argon (Fig. ), this plateau of lifetimes at high-frequency is not seen for SW silicon (Fig. 8 a).

From Fig. 8 (c) the thermal conductivity of SW silicon alloys is dominated by low-frequency modes. As seen in Fig. 5 and 8, VC-NMD and VC-ALD predict from Eq. (16) significant number of modes with  $D_{ph}(\kappa) < D_{AF,HS}$  for both LJ argon and SW silicon. However, because thermal transport in SW silicon is low-frequency dominant, the high-scatter adjustments VC-NMD\* and VC-ALD\* vary by only approximately one percent compared to the unadjusted VC-NMD and VC-ALD.

For SW silicon, bulk thermal conductivity predictions can only be made for VC-ALD and GK (Fig. 9) because of the limited system size used for VC-NMD (see Section ). For SW silicon, the thermal conductivities predicted by VC-ALD and GK are in better agreement, even without the adjustment VC-ALD\*. VC-ALD actually overpredicts by roughly 20% for  $c \geq 0.05$  compared to GK.

For LJ argon and the large concentrations and mass ratios considered in this work, the terms higher order terms are order 1 and larger at high frequencies. For SW silicon alloys the higher-order terms are also large, while good agreement is observed at all but the highest frequencies for VC-NMD and VC-ALD (Fig. 8 (a)). It is possible that higher-order interactions in the Tamura theory are also responsible for the discrepancy of the lifetimes predicted by VC-NMD and VC-ALD in SW silicon, but this discrepancy is unimportant to the overall thermal transport.

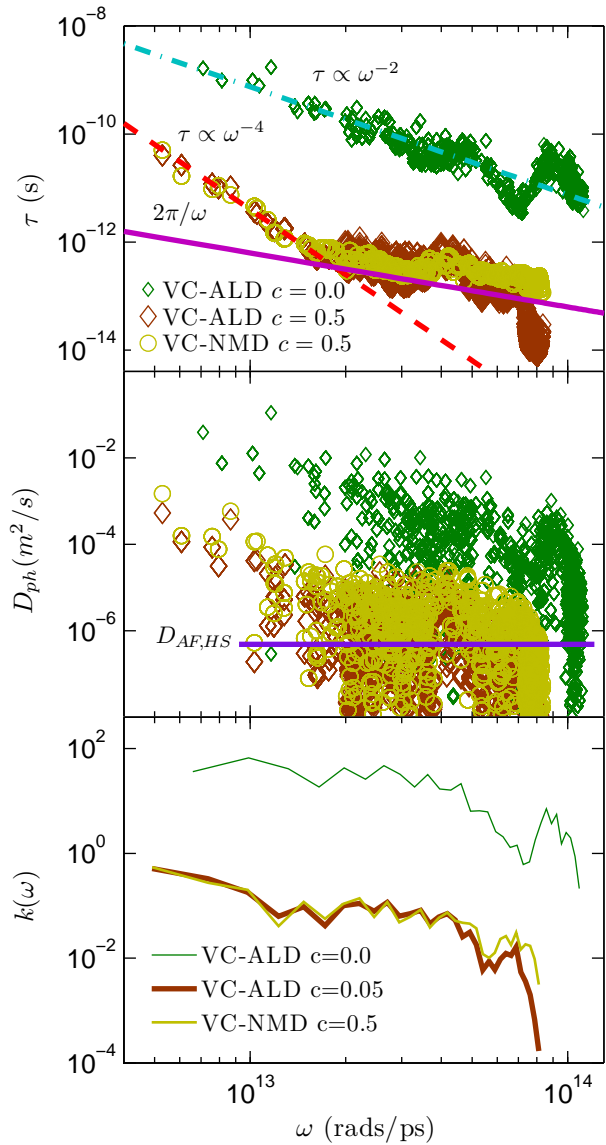


FIG. 8: (a) predicted lifetimes for VC modes using VC-NMD and VC-ALD for SW silicon. (b) predicted VC mode thermal diffusivities, compared to the AF,HS limit. (c) the thermal conductivity frequency spectrum, which is peaked at low frequency, in contrast to LJ argon (Fig. 5).

## VI. THERMAL PROPERTIES DISCUSSION

The LJ argon and SW silicon alloys studied in this work have different ranges of phonon frequencies, lifetimes, group velocities and total thermal conductivity. For bulk silicon(cite), the thermal conductivity is dominated by low-frequency modes(cite), which is also true for bulk and alloyed SW silicon (Fig. 8).(cite) For SW silicon, VC-ALD predicts thermal

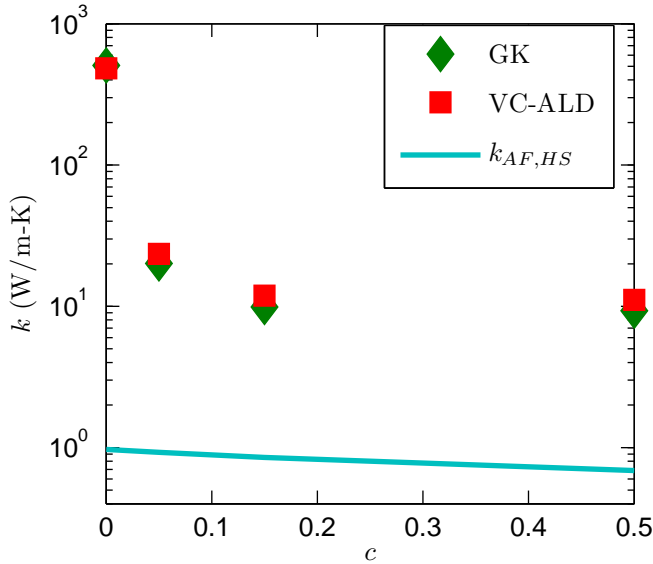


FIG. 9:

conductivities in reasonably good agreement with the explicitly disordered GK method (Fig. 9). For LJ argon, VC-ALD underpredicts the high-frequency phonon lifetimes and thermal diffusivities (Fig. 5), leading to an underprediction of thermal conductivity when compared to VC-NMD and GK (Section IV).

The results for SW silicon and LJ argon alloys suggest that the thermal modeling of ordered and disordered lattices can be separated into two broad groups: low-frequency dominated and full-spectrum materials.(cite) Materials dominated by low-frequency modes tend to have high thermal conductivities, which is due to their large group velocities and long lifetimes. (cite) These low-frequency modes follow closely the scalings predicted by the perturbative VC-ALD models, which are valid at low-frequencies.

LJ argon is a material whose thermal transport has significant contribution from high-frequency modes, even for the bulk (Fig. 5 (c)). This high-frequency range is where the perturbative Tamura theory is predicted to have non-negligible contributions from higher-order interactions (Section III C 2). While the high-order interactions in the Tamura theory are also predicted to be non-negligible for SW silicon, this does not affect the thermal conductivity predictions significantly. Even though VC-ALD underpredicts the mode lifetimes and thermal diffusivities at very high frequencies for SW silicon alloys (Fig. 8, these modes are unimportant to thermal transport. This is also true for the thermal conductivity spectrum

of SiGe alloys from first-principles predictions<sup>11</sup> and experimental measurements.<sup>29,30,62,63</sup> For example, the thermal conductivity of SiGe alloys exceeds the high-scatter limit by more than an order of magnitude at room temperature for all compositions.(cite)

The breakdown of the perturbative VC-ALD models for LJ argon is considering the thermal diffusivity of vibrational modes in the AF theory. A simple correction to the VC approximation can be made by considering a high-scatter limit for the mode specific thermal diffusivity (Section III D). This high-scatter limit is physically interpreted as vibrational modes propagating at the sound speed a distance of the lattice constant. However, the concept of a vibrational mean free path in a disordered system is only valid at low-frequencies.<sup>25,55</sup> For disordered vibrations, the lifetime and thermal diffusivity are the fundamental quantities.

For LJ argon, it is possible that the VC group velocities are an over-prediction for modes in a given interval of frequency, an effect which is compensated for by a small under-prediction of the lifetimes in the same interval of frequency when compared to Gamma-NMD (Fig. 4). The VC-NMD predicted mode lifetimes and thermal diffusivity adjusted VC-NMD\*, predict thermal conductivities in good agreement with the MD-based GK method. Based on the thermal conductivity predictions for VC-NMD\* and the well-defined peaks in the structure factors (Fig. 3), the reduction of group velocities in disordered lattices due to zone folding seems to be an underprediction of the group velocity of moderate to high frequency modes.<sup>44</sup>

## VII. SUMMARY

The concept of simple alloying remains at the forefront of efforts to control or minimize the thermal conductivity of semiconducting and thermoelectric materials (cite SiGe nanoporous, PbTe) Results in this work suggest that the lower limit for the vibrational mode thermal diffusivity in alloys is  $(1/3)v_s a$ .

The results in this work support the idea of a minimum thermal diffusivity for the vibrations in disordered lattices.(cite) Although this minimum thermal diffusivity is usually interpreted as a minimum mean free path, we find that concept is not necessary for interpreting the results of this work. The VC approximation provides a computationally cheap framework, which is essential for expensive but experimentally accurate *ab initio* methods for predicting thermal conductivity.(cite) The high-scatter limit of thermal diffusivity is more useful for examining the thermal transport in alloys under the framework of the VC

approximation. The fundamental quantity is the mode lifetimes and the group velocity is an approximation, and expressed together as thermal diffusivity they can be interpreted in the presence of disorder.

The VC approximation results in two underpredictions for modes at high frequencies: (i) underprediction of the disordered vibrational thermal diffusivities because of the VC predicted group velocities, and (ii) underprediction of the disordered mode lifetimes by the perturbative VC-ALD method. The validity of the VC approximation has been verified for SW silicon alloys, which is a model system dominated by low-frequency modes. The underprediction of both the mode group velocities by the VC and the lifetimes by VC-ALD occurs at the highest frequencies for SW silicon alloys, but these modes are unimportant to thermal transport. This is the plausible explanation for the success of the VC approximation phenomenologically and predictively for low-frequency dominated, high thermal conductivity materials.(cite)

For LJ argon alloys, which have significant thermal transport from high-frequency modes, VC-NMD and VC-ALD both underpredict the thermal conductivity compared to the system-level GK method. VC-NMD underpredicts only modestly, and can be brought into good agreement with GK by applying the high-scatter limit adjustment VD-NMD\*. For VC-ALD, the high-scatter limit adjustment VC-ALD\* still underpredicts compared to GK and VC-NMD\*, suggesting that the perturbative Tamura theory is not appropriate for LJ argon alloys. This may be true for the high-frequency modes of any disordered lattice,(cite) and the high-scatter limit  $D_{AF,HS}$  should be considered whenever the perturbative VC-ALD method is used.

## Acknowledgments

This work is supported by AFOSR award FA95501010098. This work was supported in part by a grant of computer time from the DOD High Performance Computing Modernization Program at the US Army Engineer Research and Development Center. We thank Jivtesh Garg, Zhiting Tian, Davide Donadio, Asad Hasan and Craig Maloney for helpful discussions.

## Appendix A: NMD using Non-Exact Normal Modes

For a normal mode of the lattice supercell used for the MD simulations, the autocorrelation of the total normal mode energy autocorrelations are damped exponentials with a decay time  $\tau(\nu)$  and the kinetic energy autocorrelation is a cosinusoidal exponentially-damped oscillation with frequency  $2\omega(\nu)$ . (cite AHRT) When using the VC normal modes to map the MD simulation trajectories from the explicitly disordered lattice supercells, the mode total and kinetic energy autocorrelation functions do not always follow the simple functional forms, see Fig. 10 (a) and (b). By calculating the phonon mode spectral energy  $\Phi$ , which is a phonon mode energy method in the frequency-domain,<sup>21</sup> artifacts such as multiple peaks in a given mode's energy spectrum  $\Phi$  can be observed for high concentrations,  $c = 0.5$ , Fig. 10 (a).

These artifacts in the mode energy spectrum and autocorrelations are not surprising given two considerations: (i) the MD simulations contain explicit disorder which influences the atomic trajectories, (ii) the VC normal modes are not the exact normal modes and of the explicitly disordered lattice supercells. It is important to remember that the VC normal modes are exact in the limit  $c \rightarrow 0$ .

In the case of multiple peaks in the VC phonon mode spectrum  $\Phi$ , the choice of which peak to fit to predict the phonon properties can be ambiguous. An effective lifetime can be predicted unambiguously using Eq. (11) because the VC phonon mode autocorrelations still decay to zero in a finite time, Fig. 10 (b). This result is to be expected given that the atomic trajectories contain information about the lattice energy, which from general statistical physics principles will have exponential relaxation behavior in an equilibrium ensemble.<sup>64-66</sup>

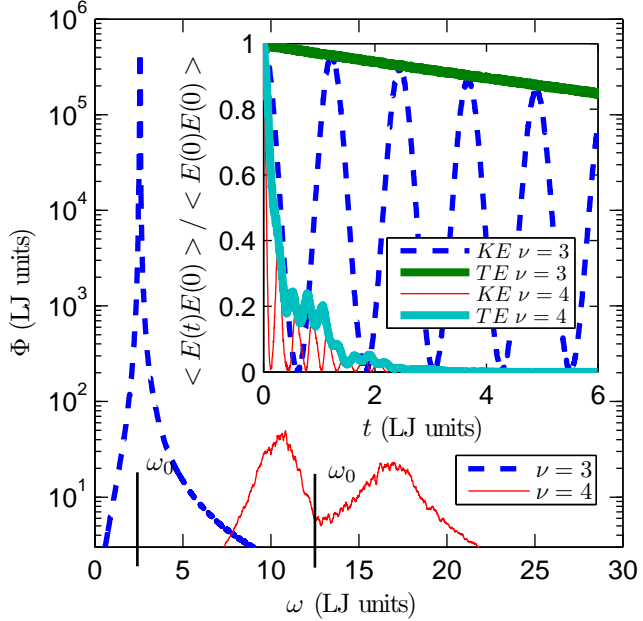


FIG. 10: The spectral energy density  $\Phi$  of two modes (polarizations  $\nu = 3, 4$  at wavevector  $[0.2 \ 0]$ ) calculated using VC-NMD for a mass disordered LJ FCC supercell ( $N_0 = 8$  and  $c = 0.5$ ). The VC dispersion-predicted peaks are labeled by  $\omega_0$ . Inset: the same mode's energy (kinetic (KE) and total (TE)) autocorrelation functions. Note the additional harmonic effects in the KE and TE autocorelation functions for  $\nu = 4$  which are due to the double peaks in  $\Phi$ . A mode lifetime can be extracted unambiguously using the integral of the TE autocorrelation function (Section III C 1).

- 
- \* Electronic address: mcgaughhey@cmu.edu
- <sup>1</sup> S.-i. Tamura, Phys. Rev. B **27**, 858866 (1983), URL <http://link.aps.org/doi/10.1103/PhysRevB.27.858>.
- <sup>2</sup> Y. K. Koh, C. J. Vineis, S. D. Calawa, M. P. Walsh, and D. G. Cahill, Applied Physics Letters **94**, 153101 (2009), URL <http://link.aip.org/link/?APL/94/153101/1>.
- <sup>3</sup> B. Qiu, H. Bao, G. Zhang, Y. Wu, and X. Ruan, Computational Materials Science **53**, 278 (2012), ISSN 0927-0256, URL <http://www.sciencedirect.com/science/article/pii/S0927025611004770>.
- <sup>4</sup> Z. Tian, J. Garg, K. Esfarjani, T. Shiga, J. Shiomi, and G. Chen, Phys. Rev. B **85**, 184303 (2012), URL <http://link.aps.org/doi/10.1103/PhysRevB.85.184303>.
- <sup>5</sup> B. Abeles, Phys. Rev. **131**, 19061911 (1963), URL <http://link.aps.org/doi/10.1103/PhysRev.131.1906>.
- <sup>6</sup> J. M. Ziman, *Electrons and Phonons* (Oxford, New York, 2001).
- <sup>7</sup> J. L. Feldman, M. D. Kluge, P. B. Allen, and F. Wooten, Physical Review B **48**, 1258912602 (1993).
- <sup>8</sup> P. B. Allen, J. L. Feldman, J. Fabian, and F. Wooten, Philosophical Magazine B **79**, 1715 (1999).
- <sup>9</sup> A. Ward and D. A. Broido, Phys. Rev. B **81**, 085205 (2010), URL <http://link.aps.org/doi/10.1103/PhysRevB.81.085205>.
- <sup>10</sup> L. Lindsay, D. A. Broido, and T. L. Reinecke, Phys. Rev. Lett. **109**, 095901 (2012), URL <http://link.aps.org/doi/10.1103/PhysRevLett.109.095901>.
- <sup>11</sup> J. Garg, N. Bonini, B. Kozinsky, and N. Marzari, Phys. Rev. Lett. **106**, 045901 (2011), URL <http://link.aps.org/doi/10.1103/PhysRevLett.106.045901>.
- <sup>12</sup> T. Shiga, J. Shiomi, J. Ma, O. Delaire, T. Radzynski, A. Lusakowski, K. Esfarjani, and G. Chen, Phys. Rev. B **85**, 155203 (2012), URL <http://link.aps.org/doi/10.1103/PhysRevB.85.155203>.
- <sup>13</sup> J. Shiomi, K. Esfarjani, and G. Chen, Physical Review B **84**, 104302 (2011).
- <sup>14</sup> K. Esfarjani, G. Chen, and H. T. Stokes, Physical Review B **84**, 085204 (2011).
- <sup>15</sup> N. d. Koker, Physical Review Letters **103**, 125902 (2009), URL <http://link.aps.org/>

- abstract/PRL/v103/e125902.
- <sup>16</sup> H. Bao, B. Qiu, Y. Zhang, and X. Ruan, Journal of Quantitative Spectroscopy and Radiative Transfer **113**, 1683 (2012), ISSN 0022-4073, URL <http://www.sciencedirect.com/science/article/pii/S0022407312002336>.
- <sup>17</sup> N. W. Ashcroft and N. D. Mermin, *Solid State Physics* (Saunders, Fort Worth, 1976).
- <sup>18</sup> F. H. Stillinger and T. A. Weber, Physical Review B **31**, 52625271 (1985).
- <sup>19</sup> R. Peierls, *Quantum Theory of Solids* (Oxford University Press, 2001).
- <sup>20</sup> D. A. McQuarrie, *Statistical Mechanics* (University Science Books, Sausalito, 2000).
- <sup>21</sup> J. M. Larkin, J. E. Turney, A. D. Massicotte, C. H. Amon, and A. J. H. McGaughey, submitted to Journal of Computational and Theoretical Nanoscience. yes, yes (2012).
- <sup>22</sup> P. B. Allen and J. L. Feldman, Physical Review B **48**, 1258112588 (1993).
- <sup>23</sup> D. Cahill and R. Pohl, Annual Review of Physical Chemistry **39**, 93121 (1988).
- <sup>24</sup> Y. He, D. Donadio, and G. Galli, Applied Physics Letters **98**, 144101 (2011).
- <sup>25</sup> J. L. Feldman, P. B. Allen, and S. R. Bickham, Phys. Rev. B **59**, 35513559 (1999), URL <http://link.aps.org/doi/10.1103/PhysRevB.59.3551>.
- <sup>26</sup> P. G. Klemens, Proceedings of the Physical Society. Section A **68** (1955).
- <sup>27</sup> P. G. Klemens, Proceedings of the Physical Society. Section A **70**, 833 (1957), URL <http://stacks.iop.org/0370-1298/70/i=11/a=407>.
- <sup>28</sup> J. Callaway, Physical Review **113**, 1046 (1959).
- <sup>29</sup> D. G. Cahill and F. Watanabe, Phys. Rev. B **70**, 235322 (2004), URL <http://link.aps.org/doi/10.1103/PhysRevB.70.235322>.
- <sup>30</sup> D. G. Cahill, F. Watanabe, A. Rockett, and C. B. Vining, Phys. Rev. B **71**, 235202 (2005), URL <http://link.aps.org/doi/10.1103/PhysRevB.71.235202>.
- <sup>31</sup> A. Skye and P. K. Schelling, Journal of Applied Physics **103**, 113524 (2008), URL <http://link.aip.org/link/?JAP/103/113524/1>.
- <sup>32</sup> W. A. Kamitakahara and B. N. Brockhouse, Phys. Rev. B **10**, 12001212 (1974), URL <http://link.aps.org/doi/10.1103/PhysRevB.10.1200>.
- <sup>33</sup> Y. Pei, X. Shi, A. LaLonde, H. Wang, L. Chen, and G. J. Snyder, Nature **473**, 66 (2011), ISSN 0028-0836, URL <http://dx.doi.org/10.1038/nature09996>.
- <sup>34</sup> K. Momma and F. Izumi, Journal of Applied Crystallography **41**, 653658 (2008), URL <http://dx.doi.org/10.1107/S0021889808012016>.

- <sup>35</sup> J. E. Turney, PhD thesis, Carnegie Mellon University, Pittsburgh, PA (2009).
- <sup>36</sup> J. V. Goicochea, M. Madrid, and C. H. Amon, Journal of Heat Transfer **132**, 012401 (2010).
- <sup>37</sup> Y. He, I. Savic, D. Donadio, and G. Galli, Phys. Chem. Chem. Phys. pp. – (2012), URL <http://dx.doi.org/10.1039/C2CP42394D>.
- <sup>38</sup> D. P. Sellan, J. E. Turney, A. J. H. McGaughey, and C. H. Amon, Journal of Applied Physics **108**, 113524 (2010).
- <sup>39</sup> A. J. H. McGaughey, PhD thesis, University of Michigan, Ann Arbor, MI (2004).
- <sup>40</sup> S. Plimpton, Journal of Computational Physics **117**, 1 (1995), ISSN 0021-9991, URL <http://www.sciencedirect.com/science/article/pii/S002199918571039X>.
- <sup>41</sup> J. D. Gale and A. L. Rohl, Molecular Simulation **29**, 291 (2003).
- <sup>42</sup> K. Esfarjani and H. T. Stokes, Physical Review B **77**, 144112 (2008).
- <sup>43</sup> L. Chaput, A. Togo, I. Tanaka, and G. Hug, Phys. Rev. B **84**, 094302 (2011), URL <http://link.aps.org/doi/10.1103/PhysRevB.84.094302>.
- <sup>44</sup> J. C. Duda, T. S. English, D. A. Jordan, P. M. Norris, and W. A. Soffa, Journal of Physics: Condensed Matter **23**, 205401 (2011), URL <http://stacks.iop.org/0953-8984/23/i=20/a=205401>.
- <sup>45</sup> A. M. Bouchard, R. Biswas, W. A. Kamitakahara, G. S. Grest, and C. M. Soukoulis, Phys. Rev. B **38**, 1049910506 (1988), URL <http://link.aps.org/doi/10.1103/PhysRevB.38.10499>.
- <sup>46</sup> A. J. H. McGaughey and M. Kaviany, in *Advances in Heat Transfer, Volume 39*, edited by G. A. Greene, Y. I. Cho, J. P. Hartnett, and A. Bar-Cohen (Elsevier, 2006), p. 169255.
- <sup>47</sup> D. Donadio and G. Galli, Phys. Rev. Lett. **102**, 195901 (2009).
- <sup>48</sup> Y. He, D. Donadio, J.-H. Lee, J. C. Grossman, and G. Galli, ACS Nano **5**, 1839\961844 (2011).
- <sup>49</sup> S. Volz and G. Chen, Physical Review B **61**, 26512656 (2000).
- <sup>50</sup> A. J. C. Ladd, B. Moran, and W. G. Hoover, Physical Review B **34**, 50585064 (1986).
- <sup>51</sup> S. N. Taraskin and S. R. Elliott, Philosophical Magazine Part B **79**, 17471754 (1999), URL <http://www.tandfonline.com/doi/abs/10.1080/13642819908223057>.
- <sup>52</sup> C. Kittel, Physical Review **75**, 974 (1949).
- <sup>53</sup> J. E. Graebner, B. Golding, and L. C. Allen, Phys. Rev. B **34**, 56965701 (1986), URL <http://link.aps.org/doi/10.1103/PhysRevB.34.5696>.
- <sup>54</sup> D. J. Ecsedy and P. G. Klemens, Phys. Rev. B **15**, 59575962 (1977), URL <http://link.aps.org/doi/10.1103/PhysRevB.15.5957>.

- <sup>55</sup> N. Xu, V. Vitelli, M. Wyart, A. J. Liu, and S. R. Nagel, Phys. Rev. Lett. **102**, 038001 (2009), URL <http://link.aps.org/doi/10.1103/PhysRevLett.102.038001>.
- <sup>56</sup> S. Shenogin, A. Bodapati, P. Kebinski, and A. J. H. McGaughey, Journal of Applied Physics **105**, 034906 (2009), URL <http://link.aip.org/link/?JAP/105/034906/1>.
- <sup>57</sup> P. Sheng, *Introduction to Wave Scattering: Localization and Mesoscopic Phenomena* (Springer, 2006), ISBN 9783540291565.
- <sup>58</sup> V. Vitelli, N. Xu, M. Wyart, A. J. Liu, and S. R. Nagel, Phys. Rev. E **81**, 021301 (2010), URL <http://link.aps.org/doi/10.1103/PhysRevE.81.021301>.
- <sup>59</sup> P. Sheng and M. Zhou, Science **253**, 539542 (1991), URL <http://www.sciencemag.org/content/253/5019/539.abstract>.
- <sup>60</sup> E. S. Landry, M. I. Hussein, and A. J. H. McGaughey, Physical Review B **77**, 184302 (2008).
- <sup>61</sup> E. S. Landry and A. J. H. McGaughey, Physical Review B **79**, 075316 (2009).
- <sup>62</sup> B. Abeles, D. S. Beers, G. D. Cody, and J. P. Dismukes, Phys. Rev. **125**, 4446 (1962), URL <http://link.aps.org/doi/10.1103/PhysRev.125.44>.
- <sup>63</sup> R. Cheaito, J. C. Duda, T. E. Beechem, K. Hattar, J. F. Ihlefeld, D. L. Medlin, M. A. Rodriguez, M. J. Campion, E. S. Piekos, and P. E. Hopkins, Phys. Rev. Lett. **109**, 195901 (2012), URL <http://link.aps.org/doi/10.1103/PhysRevLett.109.195901>.
- <sup>64</sup> G. P. Srivastava, *The Physics of Phonons* (Adam Hilger, Bristol, 1990).
- <sup>65</sup> L. Landau, E. Lifshitz, and L. Pitaevskii, *Statistical Physics, Part 2 : Volume 9*, Pt 2 (Elsevier Science & Technology Books, 1980), ISBN 9780750626361, URL <http://books.google.com/books?id=NaB7oAkon9MC>.
- <sup>66</sup> A. Rajabpour and S. Volz, Journal of Applied Physics **108**, 094324 (2010), URL <http://link.aip.org/link/?JAP/108/094324/1>.
- ††
- <sup>67</sup> For all calculations, the Lorentzian was broadened using a value of  $100\delta_{\omega,avg}$  (Section ??). For the system sizes here, the results do not differ significantly if this broadening value is varied manually or by increasing system size  $N_0$ . ‡‡
- <sup>68</sup> The Cahill-Pohl (CP) HS limit differs from the AF,HS model by a factor of approximately %20.<sup>23</sup> §§
- <sup>69</sup> For the disordered lattices studied in this work for  $c \leq 0.15$ , the predicted  $k_{AF}$  is strongly system size dependent, indicating this diverging behavior. For LJ argon alloys at  $c = 0.5$ , the

divergence with system size is small for the range of system size studied ( $N_0 = 4$  to  $N_0 = 12$ ), where  $k_{AF}/k_{GK} = 0.93$  for  $N_0 = 12$ . ¶¶

<sup>70</sup> For a finite system, the AF theory requires a broadening in frequency to predict the mode-specific thermal diffusivities. We use a Lorentzian broadening with a width of  $\delta_{\omega,avg}$ , see Section ??.

<sup>71</sup> The overprediction of thermal conductivity by VC-ALD may be related to the role of disorder in the ALD calculation.<sup>11,35</sup> While Garg et al found an overprediction of VC-ALD compared to experiment by a factor of two, the overprediction we observe in this work for SW silicon alloys is not as drastic.